An Optimized Feed-forward Artificial Neural Network Topology to Support Radiologists in Breast Lesions Classification

Vitoantonio Bevilacqua*
Dept. of Electrical and Information Engineering. Polytechnic of Bari
Via Orabona 4, 70125
Bari, Italy
vitoantonio.bevilacqua@poliba.it

Antonio Brunetti
Dept. of Electrical and Information Engineering. Polytechnic of Bari
Via Orabona 4, 70125
Bari, Italy

Maurizio Triggiani
Dept. of Electrical and Information Engineering. Polytechnic of Bari
Via Orabona 4, 70125
Bari, Italy

Domenico Magaletti
Dept. of Electrical and Information Engineering. Polytechnic of Bari
Via Orabona 4, 70125
Bari, Italy

Michele Telegrafo
Dept. of Radiology, University of Bari Aldo Moro
Piazza Giulio Cesare 11, 70120
Bari, Italy

Marco Moschetta
Dept. of Radiology, University of Bari Aldo Moro
Piazza Giulio Cesare 11, 70120
Bari, Italy

ABSTRACT

Introduction and objective: Computer Aided Decision (CAD) systems based on Medical Imaging could support radiologists in classifying malignant regions from benign ones, in the field of investigation for breast cancer detection. This decision may often follow a previous procedure dedicated to the earlier identification of Regions Of Interest (ROI) containing still unclassified lesions.

Materials and methods: Materials comprise features extracted from magnetic resonance (MR) images representing morphological properties of lesions. The Regions Of Interest identified by a previous automatic procedure validated by radiologists of the University of Bari Aldo Moro (Italy), authors of this work, 134 from 600 slices considered of interest, because they contain still unclassified damaged areas. Several techniques were tested for ROI segmentation and classification. In particular, it can be shown that the same procedures for lesioned-area discrimination were also useful for malignancy classification of lesions, themselves. In particular, MR images were processed with different image processing techniques for ROI extraction, which were, ultimately, described by morphological features, such as circularity, aspect ratio, solidity and convexity. Finally, we discuss a procedure to design a feed-forward supervised artificial neural networks (ANN) architecture based on an evolutionary strategy. In a similar approach, different ANN topologies were tested in order to find the best in terms of mean accuracy for several iterations of training, validation and test. In particular, for each topology, the training, validation and test sets were constructed using 100 random permutations of the dataset, from which the average performances were calculated.

Results: The performance of the best ANN architecture, trained using a training set of 82 samples (equally divided between malignant and benign lesions) from the 134 samples available in the whole dataset, were evaluated in terms of accuracy, sensitivity and specificity.

Conclusion: Testing determined that the supervised ANN approach is consistent and reveals good performance; in particular, the optimal ANN topology found through an evolutionary strategy showed high generalization on the mean performance indexes regardless of training, validation and test sets applied, showing good performances in terms of both accuracy and sensitivity, permitting correct classification of the true malignant lesions.

CCS Concepts

•**Computing methodologies** → **Neural networks; Genetic algorithms; Image processing;** •**Applied computing** → *Imaging;*

Keywords

Medical image classification; Artificial Neural Networks; Breast Lesions Diagnosis; Decision Support Systems

*Corresponding Author

GECCO'16 Companion, July 20-24, 2016, Denver, CO, USA

DOI: http://dx.doi.org/10.1145/2908961.2931733

1. INTRODUCTION

Nowadays, the second leading cause of death among women is breast cancer after lung tumor [1]. Advances in automated diagnostic tools allow clinicians to perform examinations of mass screening for the most common diseases, such

as breast cancer [2, 3], or polyps detection [4], where specific clinical markers help specialists in their diagnosis. Several data processing approaches in the specific medical domains are already being developed [2, 3, 5, 6, 7], due to improving effectiveness in classification and prediction networks, which significantly help clinicians in their decision making. Classification and prediction are two kinds of data analysis that can be used to extract models describing important data classes or to predict future data trends [6]. Besides the importance in finding ways to improve patients' outcomes, these computational decision support systems can reduce health costs. Moreover, several innovations in diagnostic tools for the detection of various anatomical or pathological features have been, until now, developed based on Multi-Layer Perceptron Neural Networks and Genetic Algorithms [7, 8].

Contrast enhanced magnetic resonance imaging (CE-MRI) plays an important role in the diagnosis of breast cancer with a reported sensitivity and specificity of $95-99\%$ and 80% respectively [9, 10, 11, 12, 13, 14, 15, 16, 17, 18, 19]. Image analysis is based on both morphological feature extraction and the enhancement of lesion patterns in dynamic breast MRI. This includes lesion enhancement in the early, intermediate and late post-contrast phases as depicted by means of time-signal intensity curves (TIC). The TICs are classified as steady (type I), plateau (type II) and wash-out (type III), respectively indicating benign, suspicious and malignant lesions, as in [20]. However, the not completely known biologic and patho-physiologic mechanisms of contrast named wash-in and wash-out, and the histological variability of breast lesions, explain the diverging results which have been published concerning diagnostic values of TICs [10, 20, 21]. Recent studies suggest the use of modified dynamic protocols with a reduced temporal and increased spatial resolution, compared to the standard dynamic protocol for detecting subtle morphologic details of key diagnostic importance in breast MRI [22].

Therefore, abbreviated MR protocols, including the pre-contrast and the third post-contrast THRIVE (T1-weighted high resolution isotropic volume) sequence, have been proposed in the field of breast MRI for lesion detection and characterization. In fact, in [21] the third post-contrast THRIVE sequence has been proposed; it consists of the acquisition of THRIVE sequence, 3 minutes after the contrast material injection, that is during the intermediate post-contrast period, or rather, when the wash-in phase is completed and the wash-out phase has not yet occurred. THRIVE images allow evaluation of lesion morphological characteristics with high spatial resolution, including their internal architectures and contrast enhancement. Therefore, the post-contrast image analysis mainly depends on the detection of enhancing areas, and on the evaluation of their morphology and internal architecture.

The following paragraphs are organized as follows: in Section 2 materials are described in terms of patients' characteristics, image acquisition protocol and preliminary image processing procedure regarding feature segmentation, characterization, description and quantitative evaluation. In Section 3 the methodology for the search and design of the optimal classifier is described; moreover, the strategy for reaching the best performance by the classifier itself. In Section 5 obtained results are presented, while in Section 6 the conclusions are presented.

2. MATERIALS

2.1 Patients

Between January and March 2015, 20 patients selected by the medical team, consisting of 10 diseased patients and 10 healthy ones, underwent MR examination. The twenty patients (women aged $28-77$ years; mean $\pm$ standard deviation (SD), 53.2 ± 8.9 years) have a family history of breast cancer and dense glandular structure, or have suspected breast lesions detected by mammography or ultrasonography (US), and provided informed consent according to the Declaration of Helsinki principles.

2.2 Magnetic Resonance Acquisition Protocol

MR examination was performed in the second week of the menstrual cycle in case of pre-menopausal women. In the case of a positive dynamic imaging result, histological examination provided by US-guided core needle biopsy was performed at second look US in all patients. In case of a negative result, patients were invited to resume periodic breast US examination after 6 months. MR examinations were performed on a 1.5 T MR device (Achieva, Philips Medical Systems, Best, The Netherlands) by using a four-channel breast coil.

The image acquisition protocol includes two phases during which several analyses were performed. The standard protocol consisted of:

- Transverse short TI inversion recovery (STIR) turbo-spin-echo (TSE) sequence (TR/TE/TI = 3.800/60/165 ms, field of view (FOV) = 250x450 mm (APxRL), matrix 168x300, 50 slices with 3-mm slice thickness and without gaps, 3 averages, turbo factor 23, resulting in a voxel size of 1.5 x 1.5 x 3.0 mm^3; acquisition time: 4 minutes);
- Transverse T2-weighted TSE (TR/TE = 6.300/130 ms, FOV = 250x450 mm (APxRL), matrix 336x600, 50 slices with 3-mm slice thickness and without gaps, 3 averages, turbo factor 59, SENSE factor 1.7, resulting in a voxel size of 0.75x0.75x3.0 mm^3; acquisition time: 3 minutes);
- Three-dimensional dynamic, contrast-enhanced (CE) T1-weighted high resolution isotropic volume (THRIVE) sequences (TR/TE= 4.4/2.0 ms, FOV = 250x450x150 mm (APxRLxFH), matrix 168x300, 100 slices with 4-mm slice thickness, spacing between slices: 2 mm; turbo factor 50, SENSE factor 1.6, 6 dynamic acquisitions, resulting in $1.5 - mm^3$ isotropic voxels, a dynamic data acquisition time of 1 min 30 s, and a total sequence duration of 9 min).

Gadobenate dimeglumine (Multihance, Bracco, Milan, Italy) was intravenously injected at a dose of 0.1 mmol/kg of body weight and flow rate of 1.5 ml/s followed by 20 ml of saline solution.

2.3 Description of the Images

The first phase was carried out without Contrast Medium (CM) with the following settings:

- Number of slices: 60
- Resolution of 512x512 px

- Thickness equal to 3 mm
- Gray levels with 11 bit gray-scale

After the first examination, the second phase is prepared, including six new scans, the first of which is done without CM. A contrast molecule is then given to the patient and 5 regular scans are subsequently performed every minute. It is necessary for the patient to move as little as possible in order to maintain the overlapping of the acquired slices.

In detail, this second stage was performed with the following settings:

- Number of slices: 100
- Resolution of 320x320 px
- Thickness equal to 4 mm
- 2048 Gray levels

3. METHODS

3.1 Image Registration

After capturing a significant number of slices of the same chest region at different time instances, the Image Registration procedure allows the exact superimposition of all slices. This procedure, constituted by several stages, is of utmost importance both for the human interpretation and for CAD. In detail, all images captured in the first phase and the fourth scanned in the second phase are investigated; as these are the images obtained when the contrast is more enhanced.

Unfortunately, scanned images had a different number of slices due to the different thickness of the examination; thus, a spatial matching between the two sequences was necessary in a range r = 1 mm. When slice matching was achieved, all other images were deleted, so two groups of comparable images were obtained.

A downsampling of the image depth, from 2048 gray levels to 256, was carried out executing a min - max normalization, scaling pixels in range $[0 - 255]$, and auto-adjustment of the contrast, for light isolated pixels removal. Moreover, a suitable resize, from 320 to 512 pixels, was executed for all images belonging to the second phase. Finally, all couples of images coming from the second phase were registered by means of the Rotation and Scale Translation functions in "multimode" mode.

3.2 Thorax Masking

In this CAD analysis the thoracic area was excluded from scanned images to avoid confusing the subsequent image processing phase.

For this purpose, the thorax was identified by considering a geometric parabola, which approximately follows the external border of the rib cage, characterized by three interpolation points, A, B, C, as shown in Fig. 1.

The above procedure was applied to the images acquired without CM, as they were less noisy: processing comprised executing the edge detection algorithm using the Prewitt operator [23], and then removing stray or isolated pixels.

Due to the correct execution of the acquisition protocol, all the images were correctly centered.

In order to find the limits of thoracic area, the point corresponding to the sternum had to be found. By starting from the median axis of the image, the first two intersections with the sternum, P and P' respectively, were searched; then, the first point (A) was found as the midpoint of the segment P-P' as shown in Fig. 2.

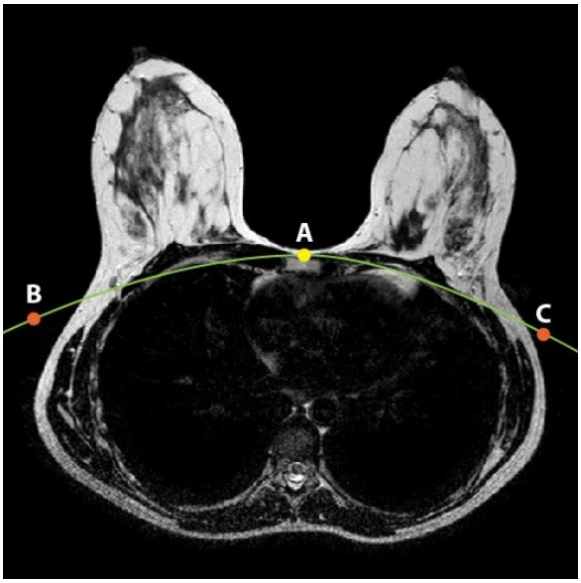

Figure 1: Interpolation of geometric parabola by means of points A, B, C

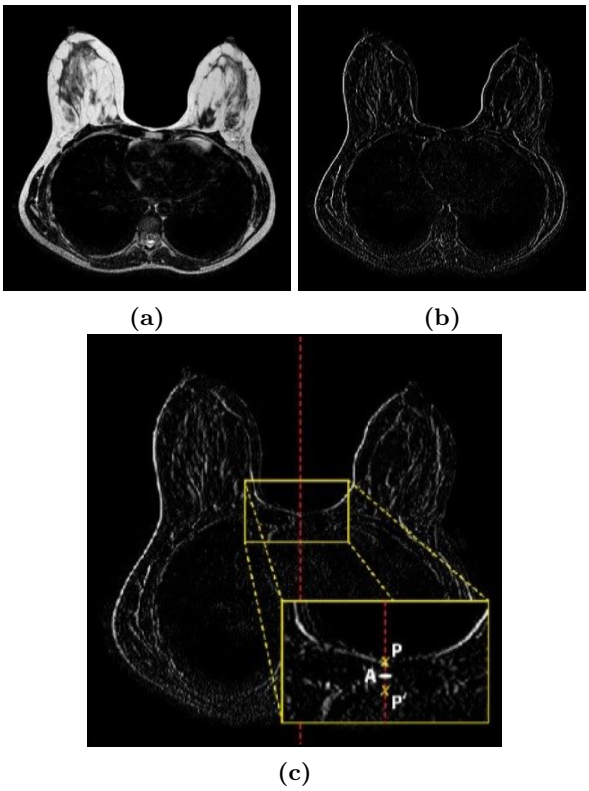

Figure 2: Processing procedure applied to an MRI: 2a Image acquired without CM; 2b Prewitt edge detection; 2c) Identification of point A as the midpoint of the segment P-P'

Moreover, in order to find points B and C, every image had to be analyzed starting from the left and right to determine point B and C respectively (Fig. 3). Each image had to be processed by columns until three adjacent light pixels were found. These pixels allow the recognition of the external lateral borders of the thorax in a point E on the left. In the same way, the external lateral point E' could be recognized on the right. The vertical segment between point A and point E could thus be evaluated and the interpolation point B was taken at 2/3 of this segment height.

The same procedure was applied to determine the interpolation point C.

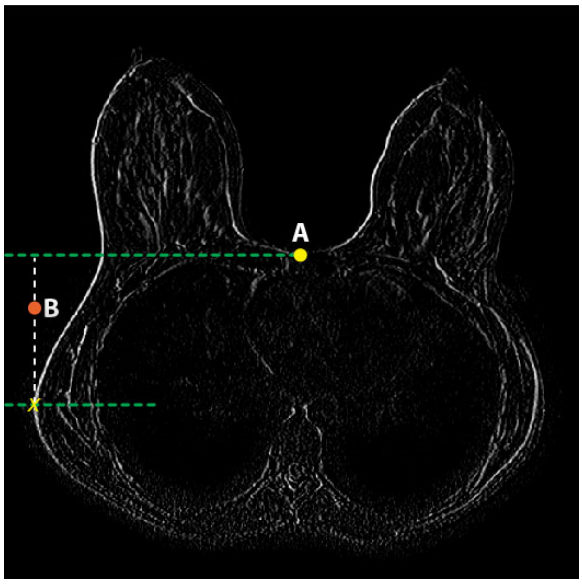

Figure 3: The algorithm representation for lateral border search.

The proposed procedure can be summarized as follows:

- starting from the pixel (0, 0) at the top left, each column of an image is processed from top to bottom, looking for 3 adjacent white pixels;
- if adjacent pixels are found, continue with the next column;
- otherwise the obtained point will represent the left end of the torso;
- move this point upwards of 2/3 of the distance between it and the point A to find the point B;
- starting from the right side, the same procedure has to be followed to find the point C;
- points A, B, C have to be interpolated as a parabola.

Then, the individuated area under the parabola can be subtracted from all images, which were previously registered and equally centered, as stated before. It can be noted that in this phase, some thoracic skin tissue was included in the final image in order to highlight any injuries. In this way, the breast area of interest was effectively isolated in order to proceed to the segmentation phase.

3.3 Image Segmentation

Since ROIs had been previously processed to remove undesired elements, the first step of this phase concerns Thresholding. Images without CM were firstly considered to find the optimal value of threshold, by using the 95th percentile of the gray level distribution, after excluding levels between $[0 - 10]$ from the image histogram.

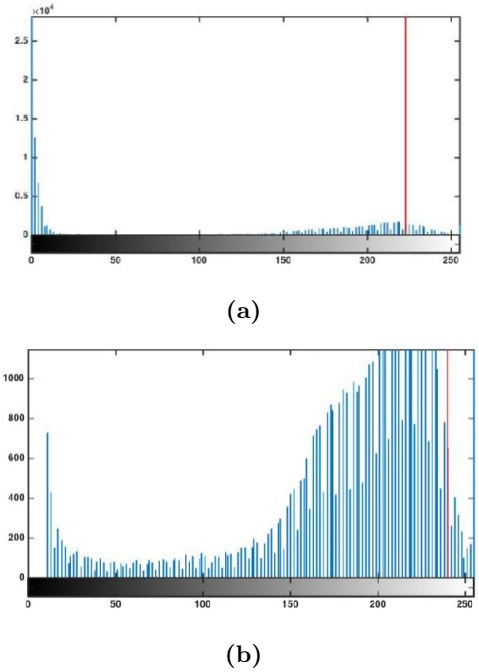

(a)

(b)

Figure 4: Image histogram with (Fig.4a) and without (Fig.4b) the pixels with gray level in range $[0 - 10]$

The removal of all very dark pixels was due to their prevalence in the histogram (Fig. 4); moreover, image darkness is also linked to the physique of each patient: more slender a patient is, the greater number of black pixels his histogram will have. Then, measurements of areas are converted from pixel space to mm^2 in order to filter all regions with a diameter lower than 5 mm. In this way, a binary mask (Fig. 5), used for images both with and without MC, were obtained.

(a) **(b)**

Figure 5: The binary mask (Fig 5b) obtained from the starting image in Fig. 5a

3.4 Feature extraction

After determining adequate ROIs in the previous steps, the following 10 features were extracted:

- F1: size in mm^2 of the suspicious lesion;
- F2, F3: average value of the gray levels of images with and without MC in ROIs, to determine areas with gray intensity different from standard ones;
- F4, F5: standard deviation value of the gray levels of images with and without MC in ROIs;
- F6: circularity expressed as $4\pi(\frac{A}{P^2})$ where A = ROI area and B = ROI perimeter;
- F7: aspect ratio intended as $\frac{majorAxis}{minorAxis}$;
- F8: eccentricity of the ellipse whose second order moments coincide with those of each ROI;
- F9: solidity, defined as ratio of the area of the ROI and the area of convex hull;
- F10: convexity (or edge roughness), given by the ratio between the perimeter of the convex hull and the one of the ROI.

While circularity and aspect ratio are used to differentiate blood vessels from other regions due to their elongated shape, solidity and convexity are useful measurements to distinguish tumor region due to the high blood vessels presence (Fig. 6), since they are indexes of the ROI roughness.

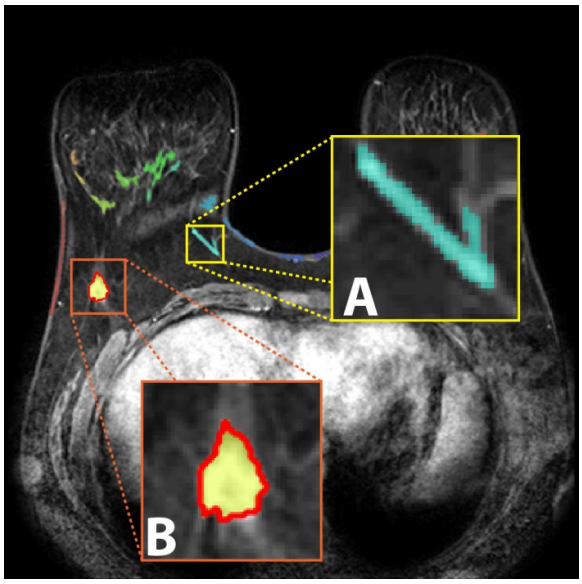

Figure 6: A (Blood Vessel): Area 68.3, Average grey value TSE/CM 196.16 / 147.23, Standard Deviation TSE/CM 29.77/30.21, Circularity: 0.24, Aspect ratio: 4.92, Eccentricity: 0.97, Solidity: 0.62, Convexity: 1.12;
B (Tumor): Area 166.35, Average grey value TSE/CM 95.66 / 203.07, Standard Deviation TSE/CM 54.53/47.34, Circularity: 0.77, Aspect ratio: 1.41, Eccentricity: 0.70, Solidity: 0.91, Convexity: 0.99

4. DETECTION AND CLASSIFICATION

Previous work has developed characterization and classification of ROIs between the ones that contain a lesion and the uninteresting ROIs. In this work, a subsequent classification step was developed for images with the presence of lesions to classify among malignant and benign lesions (Fig. 7) starting from the input pattern [F1 - F10] described in the previous section.

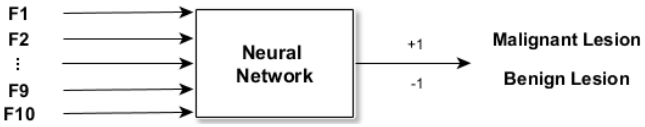

Figure 7: Block diagram of the classification process

4.1 Optimal ANN Topology Research

Neural networks are used to resolve a large variety of classification problems. In order to design a good NN classifier, many empirical rules exist in literature; despite these, some studies afforded the problem of searching the neural network optimal topology as a research problem, since some studies highlight the relationship between optimal network design and statistical model identification [24]. Moreover, the use of evolutionary algorithms for designing the optimal experimental strategy have been widely reported, e.g. in [25, 26].

Designing of a neural network could be a critical point, because a bad choice in the design phase could negatively influence the capabilities of a such classifier, such as learning or generalization.

As stated before, several approaches to research the best ANN topology could be found in the literature, for example in [8] the authors search the ANN optimal topology by using a multi-objective genetic algorithm.

In this work, the research for the optimal topology for the NN classifier was made by using a mono-objective genetic algorithm (GA), described below. A binary chromosome was assembled describing the following features of an artificial neural network:

- Number of neurons in the first hidden layer, ranging in $[1 - 256]$, coded with 8 bit;
- Number of neurons in the second hidden layer, ranging in $[0 - 255]$, coded with 8 bit;
- Number of neurons in the third hidden layer, ranging in $[0 - 255]$, coded with 8 bit;
- Activation function in the first hidden layer $[0 - 3]$, coded with 2 bit;
- Activation function in the second hidden layer $[0 - 3]$, coded with 2 bit;
- Activation function in the third hidden layer $[0 - 3]$, coded with 2 bit.

The four activation functions coded in the chromosome are the *log-sigmoid* (logsig), the *hyperpolic tangent sigmoid* (tansig), the *pure linear* (purelin) and the *symmetric saturating linear* (satlins).

The ANN features not encoded in the chromosome are fixed; in particular, the training algorithm chosen for weights

and bias update was the resilient backpropagation algorithm [27], while the activation function set in the output layer was the *hyperpolic tangent sigmoid* (tansig).

Total chromosome length is, hence, 30 bit. Operators employed in the GA set up were:

- Initial Population size equals to 100 individuals;
- Crossover with 2 points, with a probability of 0.8;
- Mutation, with a probability of 0.2;
- Selection system: elitism;
- Stop criteria set to maximum generations numbers (100), or 20 consecutive generations with fitness value unchanged;
- Fitness function = $\frac{\sum_{n=1}^{iterations} accuracy_n}{iterations}$.

As can be seen from the fitness function, GA found, as an optimal solution, the NN topology that has the highest mean accuracy after the number of iteration, which is set to 100; so each individual in the population, which corresponds to a NN topology, is trained, validated and tested 100 times and the fitness score associated with it is the mean accuracy, where each accuracy is calculated using Equation 1.

Input data, coming from the previous elaboration (see Section 3), is firstly preprocessed for normalization and balancing, as shown in the following paragraph.

4.2 Input Data and Data Preprocessing

In a preliminary step, the dataset is cleared of all uninteresting entries (e.g, areas without any kind of lesion). The resulting dataset was composed of 27 entries with a benign lesion (negatives) and 67 samples with a malignant one (positives).

It is well known that the performance of machine learning algorithms in medicine is typically evaluated using predictive accuracy, that is a measure of diagnostic ability to correctly predict the output. If the classification categories are not approximately equally represented the learning by the classifier could be compromised, since it is not useful to have unbalanced data in such a kind of problem [28]. The dataset was balanced by using the Synthetic Minority Oversampling Technique (SMOTE) [29], in order to increase the number of negative patterns until the amount of positive ones to improve the classifier learning capability. The final dataset was perfectly balanced presenting the same number of samples for each class (67 positives and 67 negatives), so a total number of 134 samples.

After smote balancing, the entire dataset was standardized using the z-score technique [30], whose aim was to rescale data absolute values in an interval centered in 0 and with a variance equal to 1.

5. RESULTS

The optimal Neural Network topology specified by the Genetic Algorithm constituted 4 layers, with 200 neurons for the first hidden layer, 64 for the second, 15 for the third and 1 neuron for the output layer. The activation functions found by the GA were *logsig* for all the hidden layers, while the *tansig* function was set for the neuron in the output layer.

The NN training, validation and test sets were obtained from the input dataset with 60% of samples for training, 20% for validation and 20% for test set. In particular, during each iteration the above sets are obtained through a random permutation of the dataset, maintaining balanced the number of samples of each class.

Moreover, the classification thresholds were determined by using Receiver Operating Characteristic (ROC) curves [31] evaluating the True Positive Rate (TPR) against the False Positive Rate (FPR) at various thresholds setting, in order to find the value able to discriminate between the two classes in the best way.

5.1 Performance Measures

Tests were performed on the optimal neural network, with 100 iterations using the same procedure previously described. In Table 1, the confusion matrix, relative to the iteration that has performed in the best way in terms of accuracy, is presented.

Predicted \ True	**Positive**	**Negative**
Positive	TP = 13	FP = 0
Negative	FN = 0	TN = 13

Table 1: Matrix Function

We utilized the following formulas to measure the performance of our classifier in terms of accuracy, specificity and sensitivity:

$$Accuracy = \frac{TP + TN}{TP + TN + FP + FN} \quad (1)$$

$$Specificity = \frac{TN}{FP + TN} \quad (2)$$

$$Sensitivity = \frac{TP}{TP + FN} \quad (3)$$

As can be seen from the previous table, an accuracy of 100%, reached with a threshold value of 0.5822; in the worst case, the value of accuracy was 73.08% (threshold value 0.4309). The resulting average indexes were 89.77% for accuracy (standard deviation = 5.84), 0.8908 for sensitivity (standard deviation = 0.1021) and 0.9046 for specificity (standard deviation = 0.0875)

6. CONCLUSIONS

In this paper we have presented a CAD system to support radiologists in classifying breast lesions from MR images. The design of a GA optimized ANN allowed us to achieve good performance in terms of a 89.77% average accuracy and 100% best accuracy.

The proposed automatic approach could be applied in clinical practice in order to differentiate benign from malignant breast lesions using CE-MRI, assisting the radiologist to classify all the detected nodules and also to exclude areas which do not require further investigations. These results are innovative in the field of breast cancer diagnosis and staging.

In the future, we can take advantage of a classification framework split in two steps: a previous intelligent individuation of ROIs and a following lesions classification. In this

way, the whole process, that starts with MR image acquisition and ends with the lesion classification could be fully automated helping the radiologists during all the phases of MR analysis.

7. AUTHOR CONTRIBUTIONS

Vitoantonio Bevilacqua and Marco Moschetta gave their contributions to the conception and design of the work. Marco Moschetta and Michele Telegrafo were responsible for the enrollments of the patients, the acquisition of MR Images, for all the clinical evaluations to set up the knowledge based and for all the interpretations of final lesions classification. Vitoantonio Bevilacqua and Maurizio Triggiani studied and performed the preliminary image processing techniques to extract the features, and Domenico Magaletti organized the data to build the pattern/target data. Vitoantonio Bevilacqua and Antonio Brunetti designed and implemented all the procedures to build the optmized classifier and Maurizio Triggiani and Domenico Magaletti gave to them contribution in the interpretation of their numerical results. All the authors contributed in drafting the work and revising it critically for important intellectual content.

8. REFERENCES

[1] US Cancer Statistics Working Group et al. United states cancer statistics: 1999–2010 incidence and mortality web-based report. *Atlanta: US Department of Health and Human Services, Centers for Disease Control and Prevention and National Cancer Institute*, 2013.

[2] William H Wolberg, W Nick Street, and Olvi L Mangasarian. Image analysis and machine learning applied to breast cancer diagnosis and prognosis. *Analytical and Quantitative cytology and histology*, 17(2):77–87, 1995.

[3] William H Wolberg, W Nick Street, and Olvi L Mangasarian. Breast cytology diagnosis via digital image analysis. *Analytical and Quantitative Cytology and Histology*, 15(6):396–404, 1993.

[4] Vitoantonio Bevilacqua. Three-dimensional virtual colonoscopy for automatic polyps detection by artificial neural network approach: New tests on an enlarged cohort of polyps. *Neurocomputing*, 116:62–75, 2013.

[5] Olvi L Mangasarian, W Nick Street, and William H Wolberg. Breast cancer diagnosis and prognosis via linear programming. *Operations Research*, 43(4):570–577, 1995.

[6] Vitoantonio Bevilacqua, Giuseppe Mastronardi, and Filippo Menolascina. Hybrid data analysis methods and artificial neural network design in breast cancer diagnosis: Idest experience. In *Computational Intelligence for Modelling, Control and Automation, 2005 and International Conference on Intelligent Agents, Web Technologies and Internet Commerce, International Conference on*, volume 2, pages 373–378. IEEE, 2005.

[7] William H Wolberg, W Nick Street, Dennis M Heisey, and Olvi L Mangasarian. Computer-derived nuclear features distinguish malignant from benign breast cytology. *Human Pathology*, 26(7):792–796, 1995.

[8] Vitoantonio Bevilacqua, Giuseppe Mastronardi, Filippo Menolascina, Paolo Pannarale, and Antonio Pedone. A novel multi-objective genetic algorithm approach to artificial neural network topology optimisation: the breast cancer classification problem. In *Neural Networks, 2006. IJCNN'06. International Joint Conference on*, pages 1958–1965. IEEE, 2006.

[9] Sylvia H Heywang-Köbrunner and Richard W Katzberg. Contrast-enhanced magnetic resonance imaging of the breast. *Investigative radiology*, 29(1):94–104, 1994.

[10] Susan G Orel, Mitchell D Schnall, Virginia A LiVolsi, and Rosalind H Troupin. Suspicious breast lesions: Mr imaging with radiologic-pathologic correlation. *Radiology*, 190(2):485–493, 1994.

[11] Wei Huang, Paul R Fisher, Khaldoon Dulaimy, Luminita A Tudorica, Brian OâĂŹHea, and Terry M Button. Detection of breast malignancy: Diagnostic mr protocol for improved specificity 1. *Radiology*, 232(2):585–591, 2004.

[12] CK Kuhl. Mri of breast tumors. *European radiology*, 10(1):46–58, 2000.

[13] F Baum, U Fischer, R Vosshenrich, and E Grabbe. Classification of hypervascularized lesions in ce mr imaging of the breast. *European radiology*, 12(5):1087–1092, 2002.

[14] Ulf Hoffmann, Gunnar Brix, Michael V Knopp, Thomas Heβ, and Walter J Lorenz. Pharmacokinetic mapping of the breast: a new method for dynamic mr mammography. *Magnetic resonance in medicine*, 33(4):506–514, 1995.

[15] Hadassa Degani, Vadim Gusis, Daphna Weinstein, Scott Fields, and Shalom Strano. Mapping pathophysiological features of breast tumors by mri at high spatial resolution. *Nature medicine*, 3(7):780–782, 1997.

[16] Susan G Orel. High-resolution mr imaging for the detection, diagnosis, and staging of breast cancer. *Radiographics*, 18(4):903–912, 1998.

[17] Paolo Belli, Melania Costantini, Enida Bufi, Andrea Magistrelli, Giuseppe La Torre, and Lorenzo Bonomo. Diffusion-weighted imaging in breast lesion evaluation. *La radiologia medica*, 115(1):51–69, 2010.

[18] Sibel Kul, Aysegul Cansu, Etem Alhan, Hasan Dinc, Gurbuz Gunes, and Abdulkadir Reis. Contribution of diffusion-weighted imaging to dynamic contrast-enhanced mri in the characterization of breast tumors. *American Journal of Roentgenology*, 196(1):210–217, 2011.

[19] Marco Moschetta, Michele Telegrafo, Leonarda Rella, Arcangela Capolongo, Amato Antonio Stabile Ianora, and Giuseppe Angelelli. Mr evaluation of breast lesions obtained by diffusion-weighted imaging with background body signal suppression (dwibs) and correlations with histological findings. *Magnetic resonance imaging*, 32(6):605–609, 2014.

[20] Edward S Fobben, Carole Z Rubin, Lester Kalisher, Alan G Dembner, Murray H Seltzer, and Elissa J Santoro. Breast mr imaging with commercially available techniques: radiologic-pathologic correlation. *Radiology*, 196(1):143–152, 1995.

[21] Christiane Katharina Kuhl, Peter Mielcareck, Sven

Klaschik, Claudia Leutner, Eva Wardelmann, JuÌÍrgen Gieseke, and Hans H Schild. Dynamic breast mr imaging: Are signal intensity time course data useful for differential diagnosis of enhancing lesions? 1. *Radiology*, 211(1):101–110, 1999.

[22] Christiane K Kuhl, Hans H Schild, and Nuschin Morakkabati. Dynamic bilateral contrast-enhanced mr imaging of the breast: Trade-off between spatial and temporal resolution 1. *Radiology*, 236(3):789–800, 2005.

[23] Judith MS Prewitt. Object enhancement and extraction. *Picture processing and Psychopictorics*, 10(1):15–19, 1970.

[24] David B Fogel. An information criterion for optimal neural network selection. *IEEE transactions on neural networks/a publication of the IEEE Neural Networks Council*, 2(5):490–497, 1990.

[25] Filippo Menolascina, Domenico Bellomo, Thomas Maiwald, Vitoantonio Bevilacqua, Caterina Ciminelli, Angelo Paradiso, and Stefania Tommasi. Developing optimal input design strategies in cancer systems biology with applications to microfluidic device engineering. *BMC Bioinformatics*, 10(S-12):4, 2009.

[26] Vitoantonio Bevilacqua, Giuseppe Mastronardi, and Giuseppe Piscopo. Evolutionary approach to inverse planning in coplanar radiotherapy. *Image Vision Comput.*, 25(2):196–203, 2007.

[27] Martin Riedmiller and Heinrich Braun. A direct adaptive method for faster backpropagation learning: The rprop algorithm. In *Neural Networks, 1993., IEEE International Conference on*, pages 586–591. IEEE, 1993.

[28] Kevin S Woods, Christopher C Doss, Kevin W Bowyer, Jeffrey L Solka, Carey E Priebe, and W Philip Kegelmeyer JR. Comparative evaluation of pattern recognition techniques for detection of microcalcifications in mammography. *International Journal of Pattern Recognition and Artificial Intelligence*, 7(06):1417–1436, 1993.

[29] Nitesh V. Chawla, Kevin W. Bowyer, Lawrence O. Hall, and W. Philip Kegelmeyer. Smote: synthetic minority over-sampling technique. *Journal of artificial intelligence research*, pages 321–357, 2002.

[30] Dennis Zill, Warren S Wright, and Michael R Cullen. *Advanced engineering mathematics*. Jones & Bartlett Learning, 2011.

[31] Andrew P Bradley. The use of the area under the roc curve in the evaluation of machine learning algorithms. *Pattern recognition*, 30(7):1145–1159, 1997.